Metall. Res. Technol. **116**, 634 (2019)

https://doi.org/10.1051/metal/2019060

&Metallurgical Research Technology

Available online at:
www.metallurgical-research.org

Regular Article

Open Access

A contribution to laser cladding of Ti-6Al-4V titanium alloy

Samar Reda Al-Sayed Ali[1,*], Abdel Hamid Ahmed Hussein[2], Adel Nofal[3], Salah Ibrahim Hassab Elnaby[1], and Haytham Elgazzar[3]

[1] National Institute of Laser Enhanced Sciences (NILES), Cairo University, 12611 Giza, Egypt
[2] Faculty of Engineering, Cairo University, 12611 Giza, Egypt
[3] Central Metallurgical Research and Development Institute (CMRDI), 11731 Helwan, Egypt

Received: 1 September 2018 / Accepted: 21 October 2019

Abstract. A wear resistant coating was successfully made on an annealed Ti-6Al-4V titanium alloy by laser surface cladding using 60 wt.% WC + wt.% 40 NiCrBSi powder blends. Coaxial laser cladding was performed by means of Yb:YAG disk laser with a 3-KW continuous wave. Different laser interaction times were attempted to get the optimal conditions for promising mechanical properties. The new contribution was to accomplish larger clad layer thickness with applying the shortest possible laser interaction time that can achieve superior clad layer properties. This will decrease energy consumption with an expected money saving which is an essential factor for successful engineering solutions. A high powder flow rate of 20 g.min^{-1} was intended in order to obtain a thick, nonporous and crack free clad layer. The clad samples were subjected to thorough microstructure investigations, in addition to microhardness and wear evaluation. The coating so produced exhibits multiple hardness values and exceptional wear resistance under adhesive/sliding wear conditions. The obtained results expose clad layer with superior quality that was achieved at a laser interaction time of 0.3 s. An enhancement in the microhardness values of the clad layers by more than fourfold was attained and the wear resistance was thus significantly improved.

Keywords: laser surface treatment / coaxial laser cladding process / laser powder cladding / laser interaction time / titanium alloy / microhardness / wear resistance

1 Introduction

Titanium alloys are broadly used as essential components in aerospace, chemical, petrochemical and marine industries thanks to their low density, high specific strength, and extraordinary corrosion resistance. Nevertheless, the service life of the titanium alloys deteriorates due to their poor wear resistance such as high friction coefficient and low abrasion wear resistance, which inhibit applying them as engineering tribological components [1,2]. One of the most effective procedures in enhancing the wear resistance of titanium alloys is the surface modification. Coatings by means of plasma spray are known to modify these alloys properties. However, wear resistance of the plasma sprayed coatings was even poorer to the original Ti-6Al-4V substrate due to the porous and loose structure of the coating [3]. Laser cladding (LC) is being currently employed to achieve this aim. The laser cladding process offers precise control of the coating on the substrate due to the high focusing of the laser beam, microstructure control, minimal substrate distortion due to confined heating with low energy input and minimal dilution with the substrate material [4–6].

Recent studies concerning the creation of a composite coating on the titanium alloys are mainly restricted to improving the hardness and abrasion wear resistance [7,8]. Ni-based alloys were usually used as a binding material for cladding of titanium alloys [9] as they exhibit superior high-temperature, wear and corrosion resistance properties, and easily adhere to the substrate. WC + Ni-based alloy powder blends were performed as metal matrix composites on several engineering materials to enhance their hardness and wear resistance [10,11]. Nonetheless, the published work concerning this cladding composite with high contents of the WC ceramic on titanium alloys is scarce. Accordingly, our recently published work [12] deals with performing a high percentage of WC coating on Ti-6Al-4V titanium alloy. This high content of WC particles aims at rising wear resistance of Ti-6Al-4V. The goal was to create a uniform distributed layer of hard WC particles that is crack-free and nonporous to enhance the wear resistance of such alloy. This was achieved by varying the laser cladding parameters (specific heat input [J.mm^{-2}]) to reach the

* Correspondence: sreda@niles.edu.eg

optimum conditions for favorable mechanical properties. A high quality clad layer was achieved at a specific heat input of 60 J.mm^{-2} with maximum clad thickness of 1 mm using powder flow rate of 6 g.min^{-1}. A microhardness level of the best clad layer reached 1195 Hv and the wear resistance was largely improved. Based on such encouraging results, the present study was carried out in order to to reach the shortest possible laser interaction time that can achieve superior clad layer properties and larger clad layer thickness. Therefore, a higher powder flow rate of 20 g.min^{-1} at the optimum specific heat input of 60 J.mm^{-2} was attempted.

2 Materials and methods

2.1 Materials

The substrate material used in this study is the commercial Ti-6Al-4V (grade 5) titanium alloy received in annealed condition. Samples of 50 mm × 30 mm × 5 mm were machined by wire cutting for the cladding process. The nominal chemical composition (wt.%) of the alloy was 6.62% Al, 3.89% V and balance Ti. A Commercial powder blend (Fig. 1) of 60% WC and 40% NiCrBSi with the chemical composition (wt.%) of 3.8C and balance W and 8.0Cr, 1.6 B, 3.5 Si, 0.3C, and balance Ni, respectively were selected as the laser cladding powder materials [13]. Particle size analysis shows that the particle size ranged from 45 to 125 μm, with a mean particle size of 90 μm.

2.2 System setup and the coaxial laser cladding process

Coaxial laser cladding was used for the fabrication of metal matrix composite coating on the Ti-6Al-4V substrate. The source of radiation is TRUDISK 3001 Yb:YAG disk laser manufactured by TRUMPF with 3 KW of maximum laser power, a 1030-nm wavelength. Argon gas was blown into the melt pool to provide shielding during the laser cladding process. Nine clad tracks were performed adjacent to each other to achieve the overlapped coating with 50% overlap. A constant specific heat input (calculated from the following equation: $Hs = P/\nu.D$, where Hs is the specific heat input (J.mm^{-2}), P is the laser power in watt, ν is the beam scanning speed in mm.s^{-1} and D is the beam diameter in mm [14]) was used with five corresponding different laser interaction times (defined as the amount of time the laser beam is in contact with material and calculated from the equation: $R = D / \nu$ where R is the laser interaction time (s), ν is the beam scanning speed in mm.s^{-1} and D is the beam diameter in mm [15]). This constant specific heat input was selected from our previous work and results of the best clad layer. A constant laser power of 1000 W was used with a range of laser beam spot sizes and laser scanning speeds in order to achieve different laser interaction times as presented in Table 1. A different laser interaction times were considered in this study for the following reasons: our literature survey on the influence of the interaction time on the cladding process suggested that this subject had been little studied and one of our objectives was to produce large clad layer thickness with superior clad layer properties while using the shortest possible laser interaction time. This will reduce energy consumption and consequently surface treatment cost.

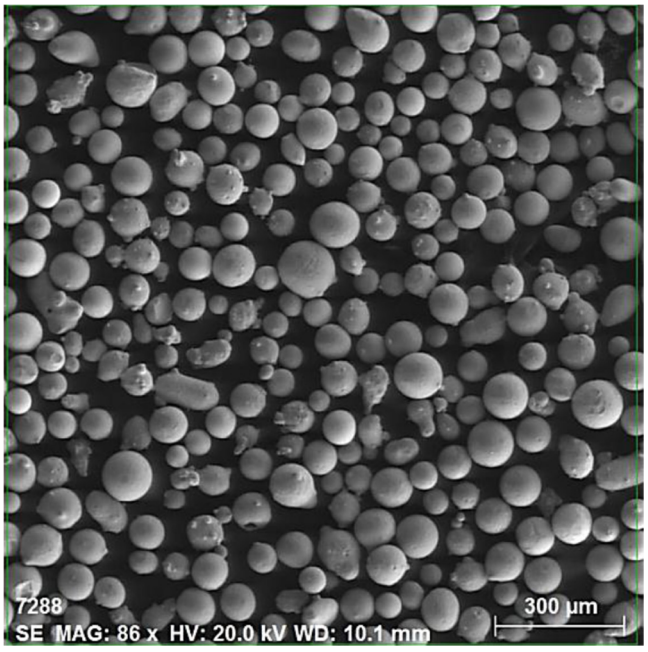

Fig. 1. SEM micrographs of the 40 NiCrBSi + 60 WC powder blend.

Microstructure examination of the laser clad composite coatings was analyzed using an Axiotech 30 optical microscope (OM) and QUANTA FEG 250 SEM attached with EDAX to analyze the chemical composition of the phases. Clad cross sections were etched with 92 mL H_2O, 6 mL nitric acid, and 2 mL hydrofluoric acid (48% concentration) [16].

2.3 Measurement of the mechanical properties

The microhardness profiles along the depth direction of the laser clad metal matrix composite coating were determined by HMV Vickers micro-hardness tester with a testing load of 980 mN and a loading time of 15 s. Wear resistance of the coating was evaluated on a TE 79 pin-on-disk type fractional and wear tribometer, where clad samples of 8 mm × 8 mm × 5 mm were used as the pins and a stainless steel alloy of diameter 100 mm and hardness of 65 HRC as the disks. The testing parameters are: normal loads = 15 N, time = 5 min and fixed sliding at speeds = 800 mm s^{-1} (150 rpm). The wear test was carried out on the top flat surface of the clad layer. A flat contact area was achieved by mechanical polishing using SiC papers and diamond cloth before the wear test.

3 Results and discussion

3.1 Initial attempts

Variables values of specific heat input with different laser interaction times were used with a constant powder feed

Table 1. Experimental conditions of laser cladding process.

Laser cladding parameters	Parameter value
Specific heat input	60 J.mm^{-2}
Powder flow rate	20 g · min^{-1}
Feeding gas	5 L · min^{-1}
Shielding gas	5 L · min^{-1}
Defocus distance	15 mm

Laser scanning speed (ν [mm.s^{-1}])	Laser beam spot sizes (D [mm])	Laser interaction time (R[s])
7.45	2.2361	0.3
5.766	2.8867	0.5
4.883	3.4156	0.7
4.3	3.8729	0.9
3.9	4.2817	1.1

rate (20 g.min^{-1}) for achieving the optimum clad layers that are free from porosities and cracks without a high dilution ratio as presented in Table 2. Range of laser interaction time values less than 0.1 s was performed. Nine tracks with 50% overlap were performed in order to cover the sample surface for the wear resistance test.

Table 2. Initial conditions of laser cladding process.

Laser cladding parameters	Parameter value
Specific heat input	6, 8, 10, 15 J.mm^{-2}
Laser interaction time for each specific heat input value	0.03, 0.05, 0.07, 0.09 s

3.1.1 Surface topography of the laser clad Ti-6Al-4V specimens

Figures 2 to 6 present the plan view of the laser clad specimens. The lowest specific heat input value (6 J.mm^{-2}) with the corresponding two different interaction times 0.03 and 0.05 s produces an unfavorable surface appearance as shown in Figure 2. Large cavities/voids and irregular powder distribution along the coated surface were observed. This cavities/voids on the cladding surface may be due to the wrong ratio of powder feed rate corresponding to laser scaning speed (underfill-type defects). In other words, there is a lack of energy.

Upon increasing in the specific heat input from 8 to 15 J.mm^{-2} (Figs. 3–5) micro cracks were detected beside the pores. The residual stress in the composites intensely affected crack creation of metal matrix coating by laser cladding process. Clad fracture is expected if the residual stress exceeds the strength of the materials [17]. The residual stresses of WC/NiCrBSi composites mainly depend on microstructure-developed stress and thermal stress. The thermal stress was induced by high temperature gradient during laser cladding process and the different coefficient of thermal expansion between WC and NiCrBSi matrix [18]. The residual stresses might not be sufficient enough for generating the cracks due to the high toughness and ductility of the titanium alloy [19]. However, during the rapid heating and cooling process of laser cladding, high temperature gradient would lead to the generation of thermal stresses in WC particle because the coefficient of thermal expansion of WC particle is lower than that of NiCrBSi based alloy.

Based on these unsuccessful trials with clad layers, longer laser interaction time above 0.1 s was attempted with the optimum specific heat input of 60 J.mm^{-2} (obtained from our recently published work [12]). There were no visible voids, inclusions, pits or cracks on the surface of clad samples as presented in Figure 6. Therefore, the best five high quality samples were chosen in order to investigate the clad structure of the Ti-6Al-4V samples and study the influence of the clad powder on the wear resistance. The best five high quality clad samples were achieved at the processing parameter as listed in Table 1. These values of laser interaction time are still lower than those listed before in our recent published work (1 and 2 s) [12].

3.2 Microstructural analysis

The microstructure of Ti-6Al-4V base metal is shown in the optical micrograph in Figure 7. The microstructure comprises two phases: equiaxed α with intergranular β of a relatively uniform grain size. Additionally, the microstructure of laser clad Ti-6Al-4V samples is shown in Figure 8, where the laser clad coatings can be separated into three zones: clad zone (CZ), interface zone (IZ) and the heat affected zone (HAZ) with a strong metallurgical bond between the clad zone and the substrate base metal, this observation is in accordance with previous studies [20]. Similar microstructures were observed in all samples regardless the difference in the laser interaction time values. The clad layer looks free from pores and cracks as well as with a mostly uniform distribution of particles in the composite matrix even when shorter laser interaction time (0.3 s) is employed. This could be due to the higher powder flow rate (20 g.min^{-1}) applied.

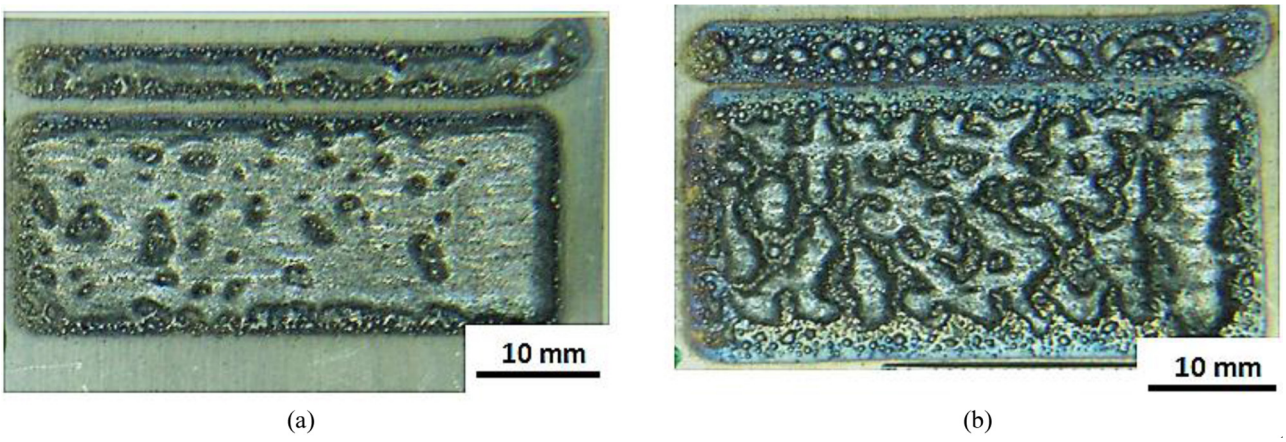

Fig. 2. Morphology of the plane view of the laser clad Ti-6Al-4V specimens processed at specific heat input = 6 J.mm^{-2} and interaction time of: (a) 0.03 s and (b) 0.05 s.

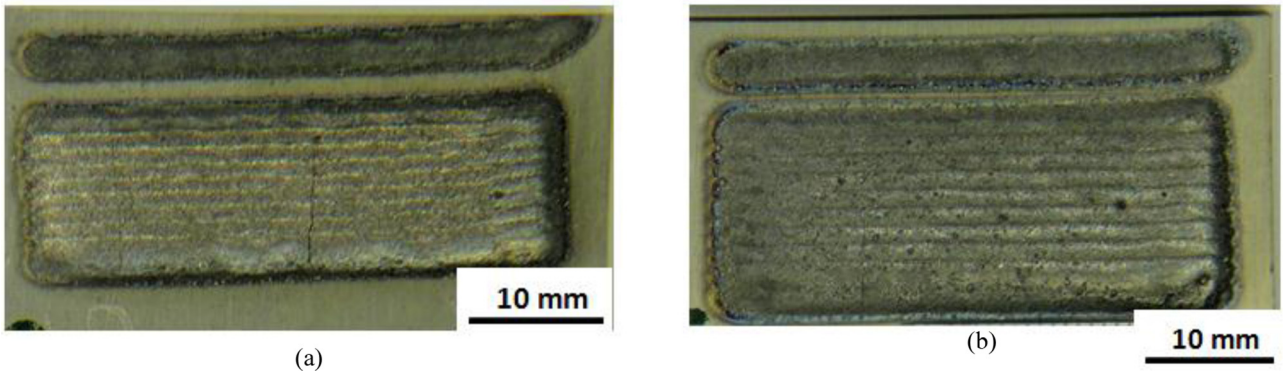

Fig. 3. Morphology of the plane view of the laser clad Ti-6Al-4V specimens processed at specific heat energy = 8 J.mm^{-2} and laser interaction times of: (a) 0.03 and (b) 0.05 s.

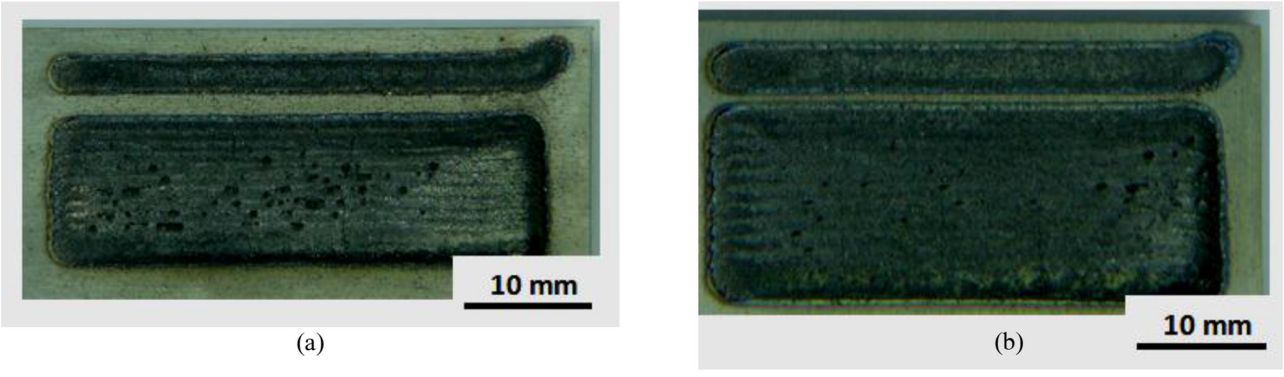

Fig. 4. Morphology of the plane view of the laser clad Ti-6Al-4V specimens processed at specific heat energy = 10 J.mm^{-2} and laser interaction times of: (a) 0.03 and (b) 0.05 s.

Additional information about the clad zone, the interface zone and the heat affected zone was obtained via SEM. The clad zone is composed of regular undissolved WC/W_2C particles dispersed in NiCrBSi matrix, as shown in Figure 9(a). The interface zone possesses a microstructure of fine dendrites plus few undissolved WC particles (Fig. 9(b)) while the HAZ exhibits acicular martensite ά-Ti as a result of the re-crystallization of the fully lamellar α+β microstructure of the substrate, as displayed in Figure 9(c). The heat affected zone (HAZ) was not perceived in samples which were processed at a lower powder flow rate (6 g.min^{-1}) (our previous work [12]) and this can be attributed to the preserved heat capacity of the powder coating due to the large amount of the deposited powder (20 g.min^{-1}). It is also commonly known that laser beam is absorbed more efficiently when the powder cloud is thicker (i.e. higher powder feed rate).

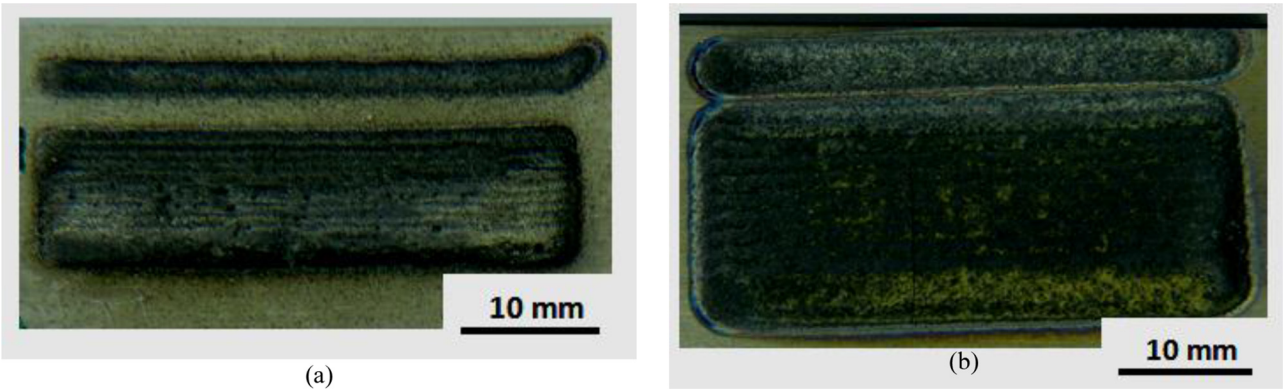

Fig. 5. Morphology of the plane view of the laser clad Ti-6Al-4V specimens processed at specific heat energy = 15 J.mm^{-2} and laser interaction times of: (a) 0.03 s and (b) 0.05 s.

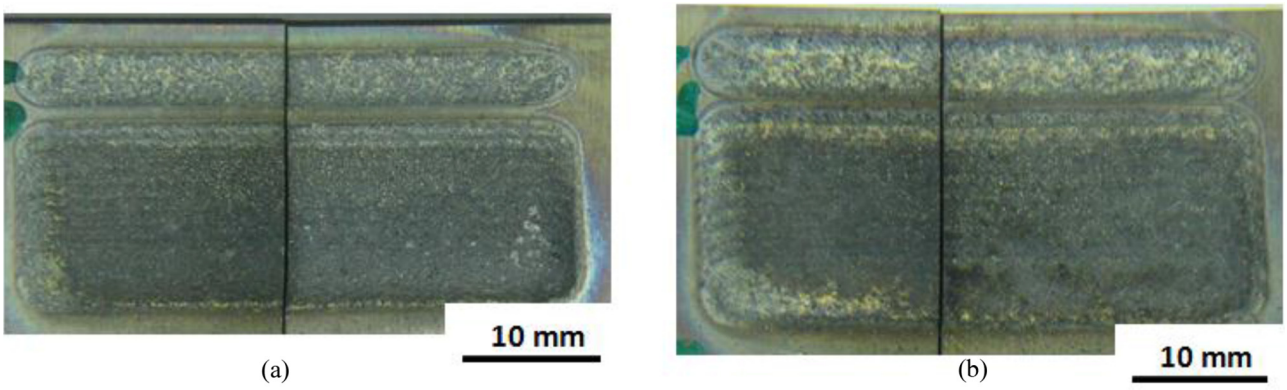

Fig. 6. Morphology of the plane view of the laser clad Ti-6Al-4V specimens processed at specific heat energy = 60 J.mm^{-2} and laser interaction times of: (a) 0.5 s and (b) 0.7 s (after wire cutting).

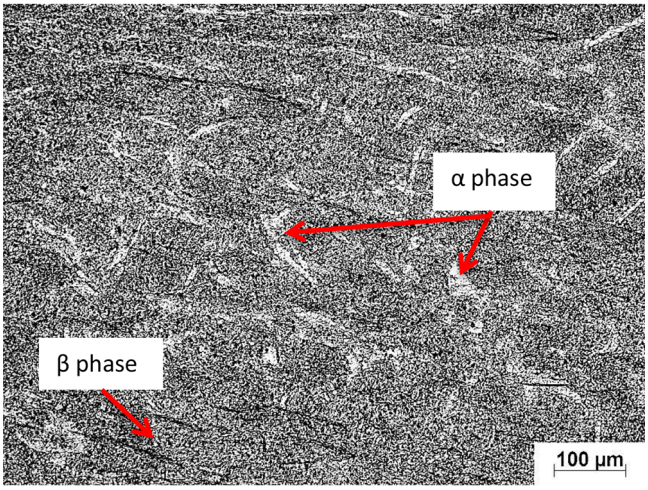

Fig. 7. Optical micrograph of the as-received Ti-6Al-4V (α phase as light regions on the micrograph while the β phase as darker regions).

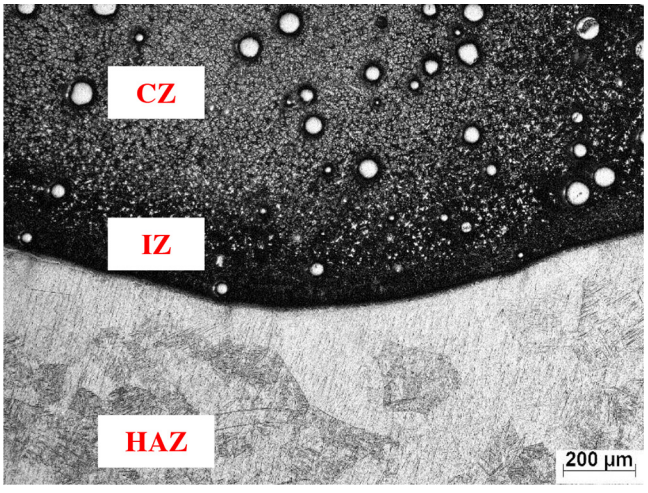

Fig. 8. Light micrographs of the cross-section of the laser clad samples processed at specific heat input of 60 J.mm^{-2} and laser interaction time of 1.1 s, clad zone (CZ), interface zone (IZ) and heat affected zone (HAZ).

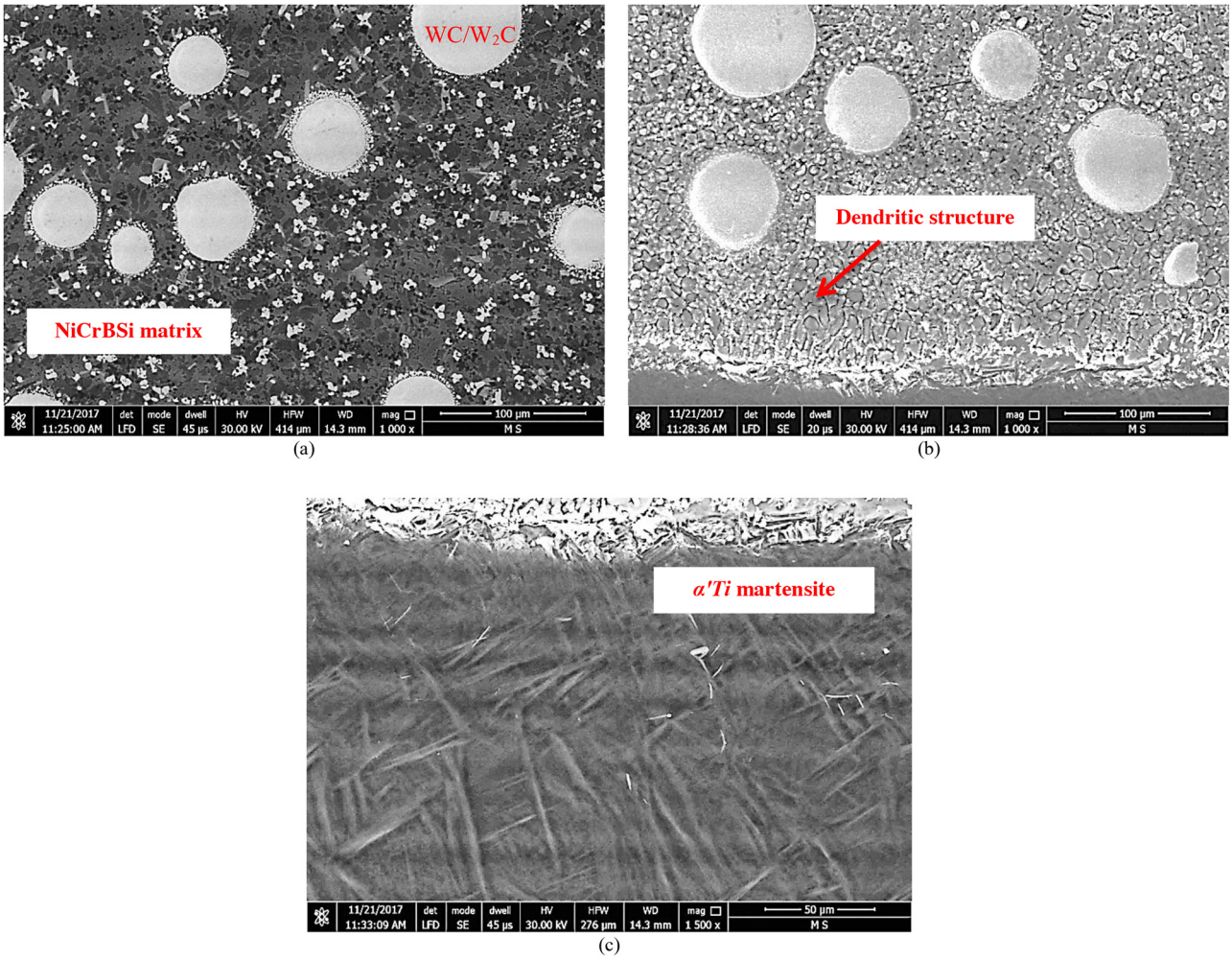

Fig. 9. SEM micrographs of sample processed at specific heat input of 60 J.mm^{-2}: (a) clad zone; (b) interface zone; and (c) HAZ.

3.3 Microstructural features of WC and TiC particles in NiCrBSi composite matrix

According to the XRD results in Figure 10, the matrix phases in the metal matrix coating layers, processed at specific heat input of 60 J.mm^{-2} mainly consisted of β-Ti, Ni, TiC, WC and W_2C. At this level of the specific heat input, there was adequate heat input level to partially dissociate the WC particles and to form TiC. These results are in accordance with Wu et al. [21], Guojian et al. [22] and Farayibi [23].

WC particles in the clad layer were further processed in order to study particle/matrix interaction. There are two different reaction layers around the WC corresponding to different laser interaction times according to the following reactions: Ti + WC; TiC + W and 2WC; W_2C + C) [18]. Figure 11(a) shows a particle with a uniform reaction layer, while Figure 11(b) shows a mixed reaction layer around the WC particle. The regular reaction layer around the reinforcement particle is observed to be 3 μm thick at short laser interaction time (0.3 s) whereas, at longer laser interaction times (0.9 and 1.1 s), the layer around the particle is characterized by mixed reaction layer with thickness of 7 μm. This may be attributed to the abundant time of heating at the longer laser interaction time which leads to more fragmentation of the WC particles from its edges and vice versa. Also, the shape of the fragmentations around the WC particles was observed to be clearly dependent on the laser interaction time.

The EDAX analysis of the dendrite structure of the interface zone shows that the matrix contains about 25 wt.% titanium (Fig. 12(a)). At lower powder flow rate of 6 g.min^{-1}, it was found that the titanium content decreased by half. The dendrite structure near the HAZ zone normally displays a higher Ti content due to the dilution of the Ti-6Al-4V substrate. The Ti content increases from 25 wt.% to 60 wt.% while the W decreases from 50 to 18 wt.%. Additionally, the EDAX analysis of the HAZ confirms that this zone contains only the main elements of the substrate Ti-6Al-4V titanium alloy (Ti, Al and V), and no existence of the other cladding elements (W, Ni and C) as shown in Figure 13.

3.4 Measurements of the clad layer, interface and HAZ thicknesses

The total clad layer thickness was evaluated by means of SEM, from the highest point of the clad zone to the deepest point of the interface zone, as typically shown in Figure 14

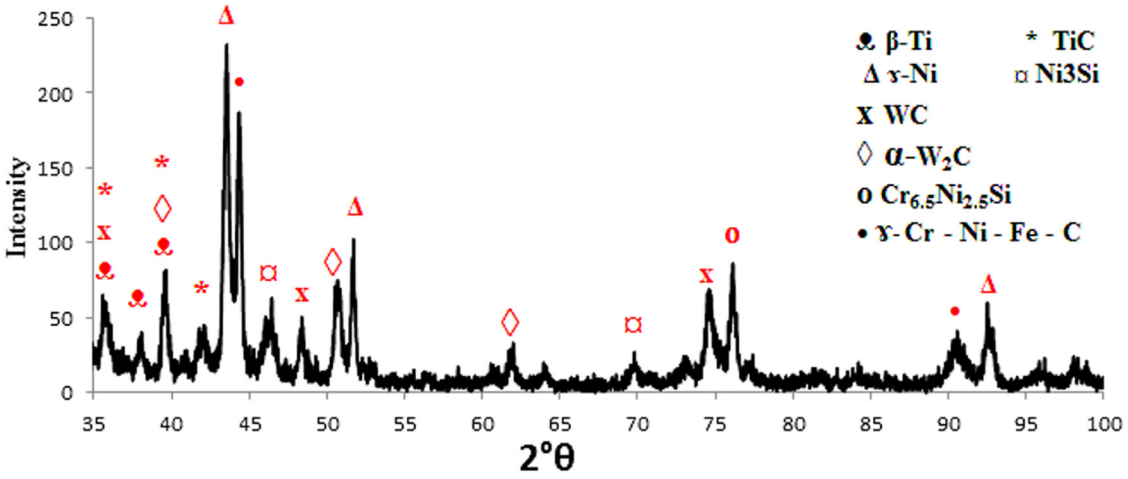

Fig. 10. X-ray diffraction spectrum of the clad layer with 60 WC + 40 NiCrBSi powder blend at specific heat input 60 J.mm^{-2} [12].

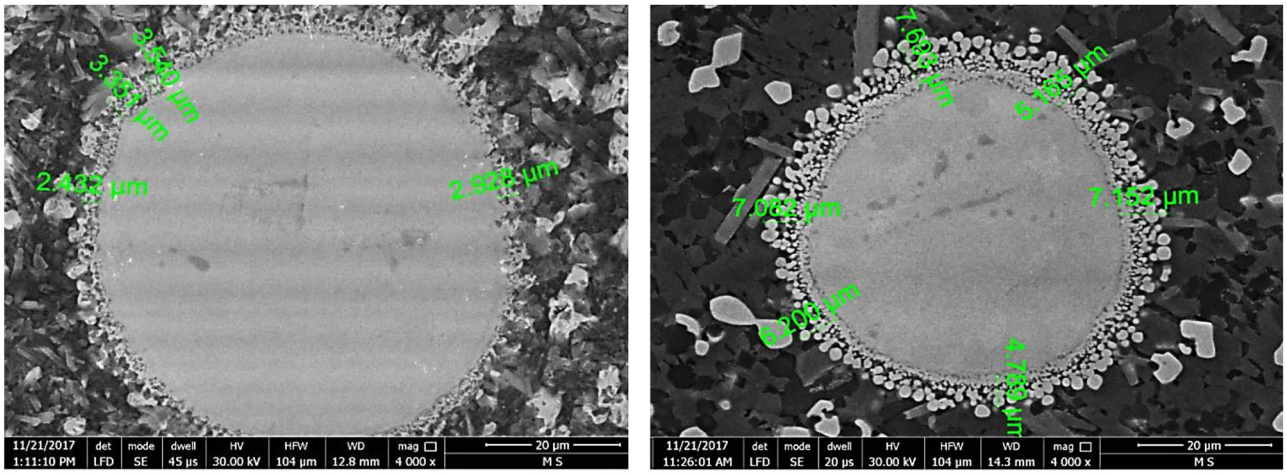

(a) (b)

Fig. 11. The reaction layer around the WC particle in case of: (a) short laser interaction time (0.3 s) and (b) long laser interaction time (1.1 s).

(a). The measured clad layer thickness value was an average of five measurements for each condition. The data obtained (Fig. 14(b)) display that the clad thickness increases with the increase in the laser interaction time. The obtained thickness of the shallowest clad layer was 2.077 mm and was associated with the shortest laser interaction time (0.3 s), while the deepest clad thickness was 2.41 mm and was achieved with the longest laser interaction time (1.1 s). The obtained clad thicknesses at all selected laser interaction times are thicker than those previously reported in other studies [24]. Additionally, at the same specific heat input (60 J.mm^{-2}) our earlier study [12] records only a 1-mm clad thickness at the powder flow rate of 6 g.min^{-1} in comparison to the present 2.41 mm clad thickness at the higher powder flow rate of 20 g.min^{-1}. The total clad thickness recorded in this paper was 2.4 mm corresponding to the higher powder feed rate of 20 g.min^{-1}. It is recalled that a corresponding 1-mm was obtained in earlier study at the powder feed rate of 6 g.min^{-1}.

Furthermore, the thickness of the interface zone and the HAZ were measured and both of their thicknesses were found to increase with the laser interaction time. Increasing laser interaction time increases the interface zone thickness from 308 to 472 µm which affects the added matter thickness (deposited material) as presented in Figure 15. The HAZ thickness also significantly increases from 1.361 to 2.474 mm when the laser interaction time is increased from 0.3 to 1.1 s.

3.5 Dilution ratio and microhardness distribution

3.5.1 Dilution ratio

The dilution ratio was calculated based on the clad layer geometry [25,26]. It is known as the ratio of the clad depth below the substrate (D_c) divided by the summation of the clad height and the clad depth (T_c), according to the equation: $D_R = D_c/T_c$. Figure 16 clarifies that the dilution ratio of the laser clad layer increases with the increase in the laser interaction time. This can be attributed to the

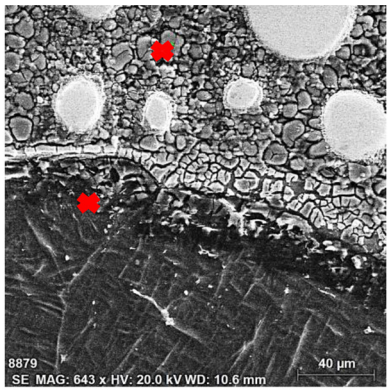

Element	W	Ti	Ni	C	V
Weight percent %	52.46	25.71	11.58	9.51	0.75

(a)

Element	Ti	W	Ni	Al	C	Cr
Weight percent %	61.14	17.91	8.53	5.38	4.39	2.65

(b)

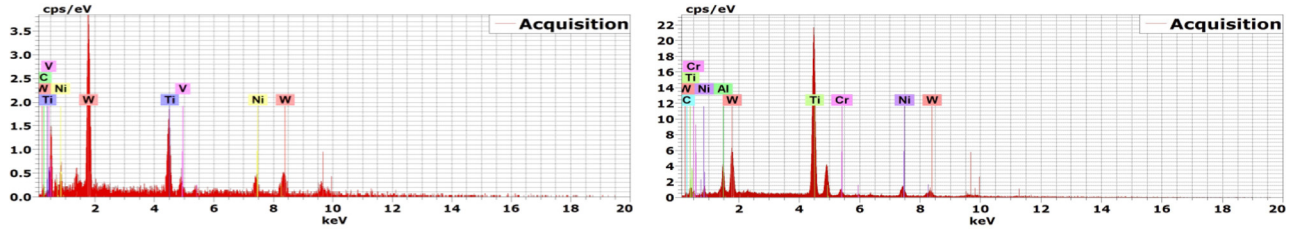

(a) (b)

Fig. 12. EDX analysis of the dendritic structure of the interface zone for sample processed at laser interaction time of 1.1 s. (a) far from the HAZ; (b) near the HAZ.

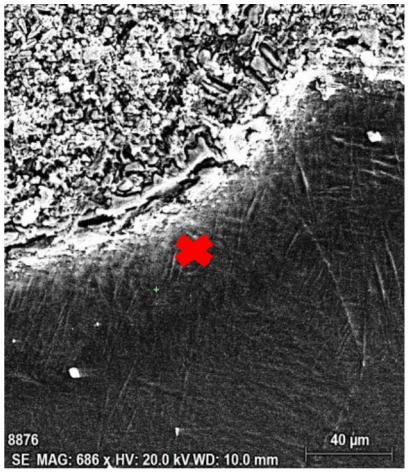

Element	Ti	Al	V
Weight %	88.32	7.78	3.9

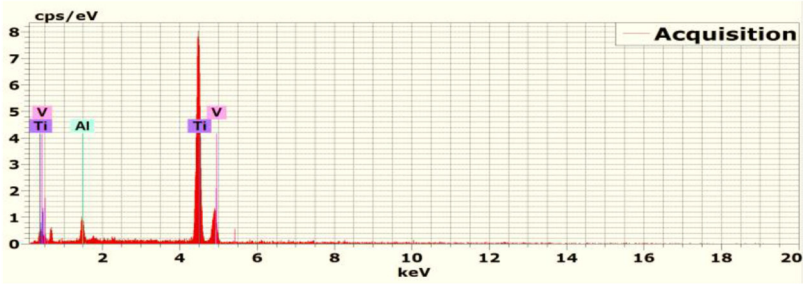

Fig. 13. EDAX analysis of the HAZ of samples processed at laser interaction time of 0.3 s.

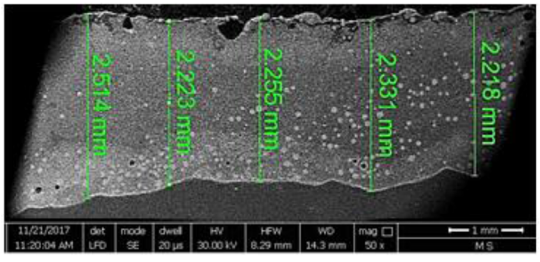

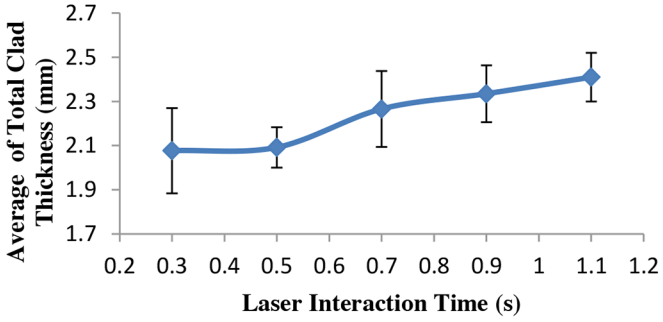

(a) (b)

Fig. 14. (a) Measurement of the clad thickness; (b) clad thickness vs. the laser interaction time.

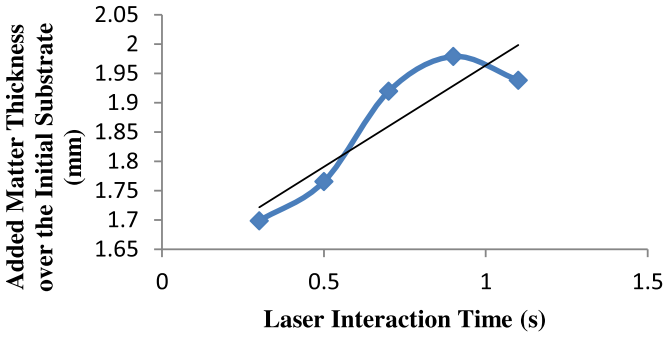

Fig. 15. The added matter thickness vs. the laser interaction time.

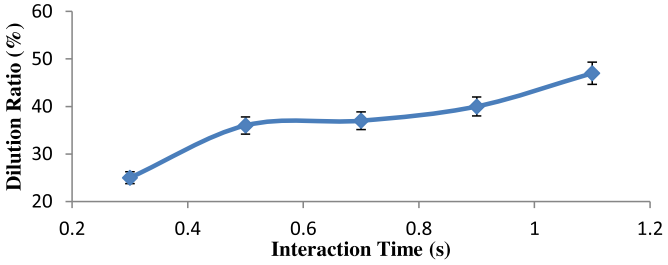

Fig. 16. Dilution ratios versus the laser interaction time (s).

decrease in the supplied laser energy with the short interaction time and vice versa. Least dilution ratio was accompanying to the shortest laser interaction time (0.3 s).

The clad weight (M) was calculated as presented in Table 3. Obviously, the clad weight increased with laser interaction time indicating more energy absorption by the powder. Hence, both the clad layer thickness and dilution ratio were increased. However, the minimum layer thickness ranged from 2 to 2.4 mm while the dilution ratio varied in larger proportions, from 25 to 47%.

3.5.2 Microhardness distribution

Figure 17 displays the variation of microhardness across the clad sections as well as the starting alloy. The clad zones have the highest values microhardness. A step decrease in the hardness values from clad zone towards the substrate due to the difference in microstructure. These results are observed in all conditions of different laser interaction times. The microhardness of composite matrix lies between 1200–1900 HV0.1. Clearly, the hardness level increases by 3–4 times down to ~2 mm below the surface contrasting the 400 μm at the lower powder flow rate (6 g.min^{-1}). This is attributed to the further preservation of the large amount WC particles in the NiCrBSi matrix due to the higher amount of the powder feeding rate (20 g.min^{-1}). This is also besides the uniform distribution of TiC clusters along the clad layer due to the appropriate combination between the specific heat input and laser interaction time. The mean microhardness of the composite matrix is 1384, 1361, 1450, 1358, and 1425 HV0.1 for samples processed at the laser interaction times of 0.3, 0.5, 0.7, 0.9, 1.1 s, respectively. Normally, high hardness values refer to measurements that have been carried at the boundaries

Table 3. The calculation of clad weight.

Laser interaction time	Speciment weight before cladding process (M1) (g)	Speciment weight after cladding process (M2) (g)	Clad weight (M) (g)
0.3	33.12	38.33	5.21
0.5	34.68	41.08	6.4
0.7	32.22	38.80	6.58
0.9	33.18	40.87	7.69
1.1	33.84	41.84	8

or inside the WC particles and therefore, they were excluded from presentation in Figure 17. Otherwise, the interface zones hardness values ranges from 950 to 1100 HV0.1. The reduction in the hardness at the interface zone is clearly associated with the presence of the dendritic structure with fewer numbers of the WC particles as well as the influence of the dilution of the clad region content with Ti-6Al-4V substrate material. Finally, the recrystallized regions of the substrate in the HAZ have hardness value range of 680–418 HV0.1. This hardness level is close to double the hardness level of the unaffected region of the substrate. This is a consequence of the presence of the ά-Ti martensitic structure as a result of the localized metallurgical change due to rapid heating and cooling and those high hardness values are similar to values reported in the literature [27]. It is to be noted that present values were obtained under a load of 980 mN and the expected rapid heating and quenching induced by laser re-melting process can elevate the micro-hardness of α'-Ti martensite obtained.

Hardness indentations near the embedded WC particle and along the HAZ are displayed in Figure 17. The elevation of in the hardness values near the WC particle inside the clad matrix is due to the interdiffusion and microstructure modification around the particles and the large amount of WC and TiC clusters along the clad zone. The ratio of the composite matrix mean hardness to the embedded WC particle hardness is ~1:2.4. While large hardness indentation was observed to be in the HAZ due to the lower hardness values in this zone (Fig. 18(c)).

3.6 Wear resistance of the laser clad samples

The primary purpose of producing WC/NiCrBSi composite on Ti-6Al-4V alloy substrate via laser cladding is to improve its wear resistance. After laser cladding, the wear resistance of the laser clad layers was increased which is in accordance with previous studies [21–23]. From Figure 19, the weight loss of the best laser clad sample (0.0027 g) is significantly less than that of the as-received Ti-6Al-4V sample (0.781 g) (i.e. ~ 0:4%) which reflect the remarkably higher wear resistance as a result of laser cladding. In addition, the weight loss of samples processed at short laser interaction time (0.3 s) is less than that processed at the longer interaction time (1.1 s) (0.0027 g vs. 0.0037 g). This may be due to the increased dilution with the titanium substrate in the case of the longer interaction time of laser with the samples (dilution ratio of 25% vs. 47%).

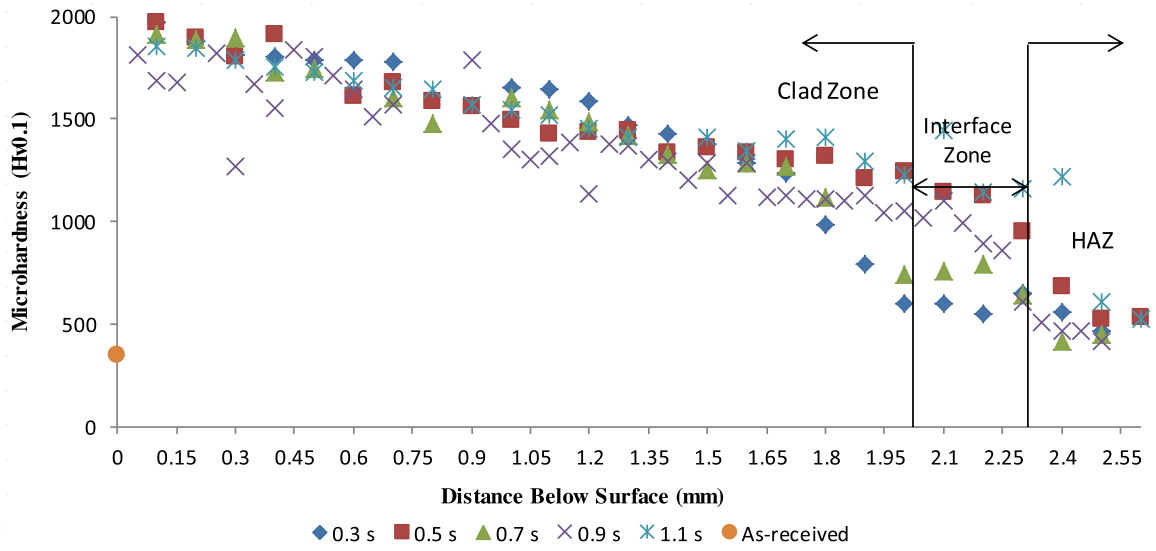

Fig. 17. Microhardness profiles of samples processed versus the distance below surface for different laser interaction time.

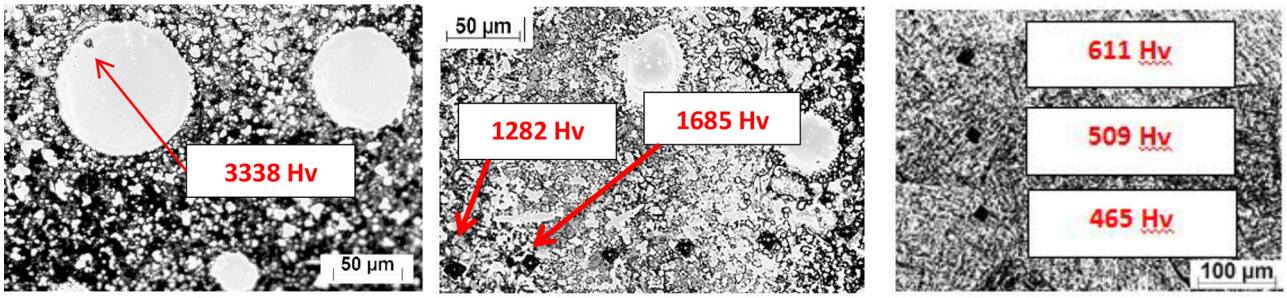

Fig. 18. Microhardness indentations. (a) Inside the WC particle; (b) the composite matrix; (c) along the HAZ.

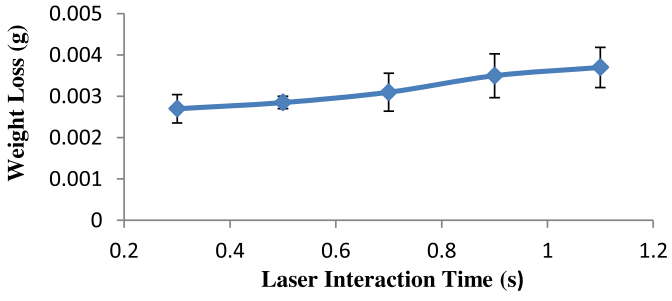

Fig. 19. Clad layer weight loss versus laser interaction time.

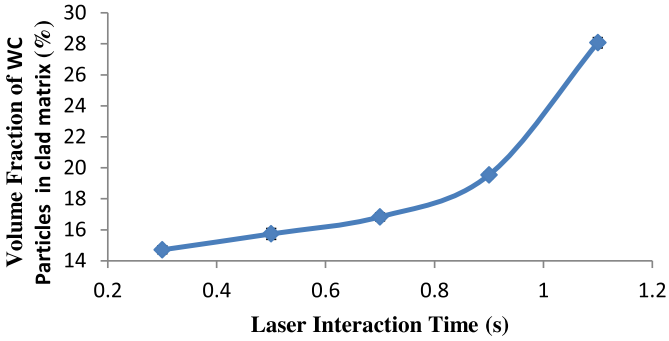

Fig. 20. Volume fraction of the carbide particles vs. laser interaction time.

Additional factor that may influence the wear resistance results is the volume fraction of the WC particles in the clad matrix. Therefore, the volume fraction of the WC particles was determined and plotted versus the laser interaction time as presented in Figure 20. The general trend is an increase in the WC volume fraction (14.7 to 28%) with the increase in laser interaction time 0.3 and 1.1 s, respectively. In spite of the lower volume fraction of WC particles that corresponds to the laser interaction time of 0.3 s, high hardness values of the clad layer were obtained. This may be due to the preservation of WC particles in the clad matrix. The fact that the WC particles were partially dissolved during the prolonged laser interaction time may be the reason for the reduction in the wear resistance of the clad layer.

The enhanced wear resistance of the metal matrix composite coating depends on several factors. These factors may include: a uniform distribution of the reinforcement (WC and TiC), high fraction of the reinforcement in the

composite matrix due to high powder feeding rates and composite without cracks and pores [28]. Additionally, microhardness of the laser clad composite is an important factor to be considered. In this study, an improvement in the microhardness values (for example, 1450 vs. 350 HV of the base alloy) was achieved; i.e. more than fourfold increase of the hardness after laser cladding.

4 Conclusions

(1) A (60% WC–40% NiCrBSi) metal matrix composite layer was successfully deposited on Ti-6Al-4V alloy by coaxial laser cladding using Yb:YAG disk laser with laser interaction time values ranges from 0.3 to 1.1 s. (2) Laser interaction time values below 0.1 s were found insufficient for producing good quality of clad samples. (3) The achieved clad layer was divided into three zones based on dissimilar microstructures: clad, interface and HAZ zones. The clad zone is mainly composed of undissolved WC and TiC particles embedded in NiCrBSi metal matrix while the interface zone displays a fine dendritic structure with few undissolved WC particles. The third zone (HAZ) with its acicular martensitic structure was not perceived in samples processed at lower powder flow rate ($6\,g.min^{-1}$). (4) By means of the high powder flow rate ($20\,g.min^{-1}$), the clad thickness is increased more than twice that resulting from lower powder flow rate ($6\,g.min^{-1}$). (5) A high microhardness gain (for example, 1450 vs. 350 HV of the base alloy) is achieved; the hardness values of the surface after laser cladding were enhanced by more than four fold. Also, the HAZ hardness values range from 418 to 680. (6) The wear resistance after the laser cladding process was significantly enhanced by ~250 times over that recorded for the as-received samples and the weight loss was found to be directly dependent on the dilution ratio. (7) An optimization of the laser cladding process corresponds to the lowest laser interaction time (0.3 s) which results in a high quality of clad layer with uniformly dispersed of WC particles in the NiCrSiB matrix, and nonporous crack free layer. It exhibits a high average microhardness value (1384 HV) and exceptional improvement in the wear resistance, as a result of the lowest dilution ratio (25%) with the titanium alloy substrate. This laser interaction time value (0.3 s) is less than half the laser interaction time value (1 s) that was achieved in our previous study which means a reduction in energy consumption by more than half.

Acknowledgments. The authors gratefully acknowledgment the cooperation of The Institut für Werkzeugmaschinen und Fertigung, Departement Maschinenbau und Verfahrenstechnik, ETH Zürich, Switzerland.

References

1. G. Kartal, S. Timur, M. Urgen, A. Erdemir, Electrochemical boriding of titanium for improved mechanical properties, Surf. Coatings Technol. **204**, 3935–3939 (2010). DOI: 10.1016/j.surfcoat.2010.05.021
2. J. Li, C. Chen, T. Squartini, Q. He, A study on wear resistance and microcrack of the Ti3Al/TiAl + TiC ceramic layer deposited by laser cladding on Ti-6Al-4V alloy, Appl. Surf. Sci. **257**, 1550–1555 (2010). DOI: 10.1016/j.apsusc.2010.08.094
3. H.M. Wang, Y.F. Liu, Microstructure and wear resistance of laser clad Ti5Si3/NiTi2 intermetallic composite coating on titanium alloy, Mater. Sci. Eng. A **338**, 126–132 (2002). DOI: 10.1016/S0921-5093(02)00076-X
4. J.C. Ion, Laser processing of engineering materials: principles, procedure and industrial application, Boston, 2005, ISBN 9780750660792
5. S.H. Mok, G. Bi, J. Folkes, I. Pashby, Deposition of Ti − 6Al − 4V using a high power diode laser and wire, Part I: investigation on the process characteristics, 2015. DOI: 10.1016/j.surfcoat.2008.02.008
6. A.K. Sachdev, K. Kulkarni, Z.Z. Fang, R. Yang, V. Girshov, Titanium for automotive applications: challenges and opportunities in materials and processing, JOM **64**, 553–565 (2012). DOI: 10.1007/s11837-012-0310-8
7. C. Zhang, M. Fujii, Tribological behavior of thermally sprayed WC coatings under water lubrication, Mater. Sci. Appl. **7**, 527–541 (2016). DOI: 10.4236/msa.2016.79045
8. R. Song, J. Li, J.Z. Shao, L.L. Bai, J.L. Chen, C.C. Qu, Microstructural evolution and wear behaviors of laser cladding Ti2Ni/α (Ti) dual-phase coating reinforced by TiB and TiC, Appl. Surf. Sci. **355**, 298–309 (2015). DOI: 10.1016/j.apsusc.2015.07.131
9. B.R. Haldar, P.S. Agarwal, Laser cladding of in-situ TiB, TiC and TiN reinforced Ni-Ti MMC coating on Ti-6Al-4V for improving tribological performance. 4th Int. 25 All india Manuf. Technol. Des. Res. 2012, pp. 796–801
10. J.A. Varela, J.M. Amado, M.J. Tobar, M.P. Mateo, A. Yañez, G. Nicolas, Characterization of hard coatings produced by laser cladding using laser-induced breakdown spectroscopy technique, Appl. Surf. Sci. **336**, 396–400 (2015). DOI: 10.1016/j.apsusc.2015.01.037
11. M.R. Amaya-Vazquez, J.M. Sánchez-Amaya, Z. Boukha, F. J. Botana, Microstructure, microhardness and corrosion resistance of remelted TiG2 and Ti6Al4V by a high power diode laser, Corros. Sci. **56**, 36–48 (2012). DOI: 10.1016/j.corsci.2011.11.006
12. S. Al-Sayed Ali, A. Hussein, A. Nofal, S. Hasseb Elnaby, H. Elgazzar, H. Sabour, Laser powder cladding of Ti-6Al-4V α/β alloy, Materials (Basel) **10**, 1178 (2017). DOI: 10.3390/ma10101178
13. Oerlikon Group − Balzers, Metco, Barmag, Neumag, Graziano, Fairfield «Oerlikon Corporate», available online: https://www.oerlikon.com/en/ (accessed on Sep 14, 2017)
14. W.M. Steen, J. Mazumder, Laser material processing, 4th ed., Springer, UK, 2010, ISBN 978-1-84996-061-8
15. A.N. Samant, S.P. Harimkar, N.B. Dahotre, Laser beam operation mode dependent grain morphology of alumina, J. Appl. Phys. **102**, 0–6 (2007). DOI: 10.1063/1.2825403
16. Metallographic Etching. Available online: http://www.metallographic.com/Technical/Etching.htm (accessed on Jan 7, 2017)
17. P.B. Kadolkar, T.R. Watkins, J.T.M. De Hosson, B.J. Kooi, N.B. Dahotre, State of residual stress in laser-deposited ceramic composite coatings on aluminum alloys, Acta Mater. **55**, 1203–1214 (2007). DOI: 10.1016/j.actamat.2006.07.049

18. S. Zhou, X. Zeng, Q. Hu, Y. Huang, Analysis of crack behavior for Ni-based WC composite coatings by laser cladding and crack-free realization, Appl. Surf. Sci. **255**, 1646–1653 (2008). DOI: 10.1016/j.apsusc.2008.04.003
19. C. Lee, H. Park, J. Yoo, C. Lee, W. Woo, S. Park, Residual stress and crack initiation in laser clad composite layer with Co-based alloy and WC+NiCr, Appl. Surf. Sci. **345**, 286–294 (2015). DOI: 10.1016/j.apsusc.2015.03.168
20. R.L. Sun, Y.W. Lei, W. Niu, Laser clad TiC reinforced NiCrBSi composite coatings on Ti-6Al-4V alloy using a CW CO_2 laser, Surf. Coatings Technol. **203**, 1395–1399 (2009). DOI: 10.1016/j.surfcoat.2008.11.012
21. P. Wu, C.Z. Zhou, X.N. Tang, Microstructural characterization and wear behavior of laser cladded nickel-based and tungsten carbide composite coatings, Surf. Coatings Technol. **166**, 84–88 (2003). DOI: 10.1016/S0257-8972(02)00730-2
22. G. Xu, M. Kutsuna, Z. Liu, L. Sun, Characteristic behaviours of clad layer by a multi-layer laser cladding with powder mixture of Stellite-6 and tungsten carbide, Surf. Coatings Technol. **201**, 3385–3392 (2006). DOI: 10.1016/j.surfcoat.2006.07.210
23. P.K. Farayibi, J. Folkes, A. Clare, O. Oyelola, Cladding of pre-blended Ti-6Al-4V and WC powder for wear resistant applications, Surf. Coatings Technol. **206**, 372–377 (2011). DOI: 10.1016/j.surfcoat.2011.07.033
24. J.L. Chen, J. Li, R. Song, L.L. Bai, J.Z. Shao, C.C. Qu, Effect of the scanning speed on microstructural evolution and wear behaviors of laser cladding NiCrBSi composite coatings, Opt. Laser Technol. **72**, 86–99 (2015). DOI: 10.1016/j.optlastec.2015.03.015
25. A.I. Noskov, A.K. Gilmutdinov, R.M. Yanbaev, Effect of coaxial laser cladding parameters on bead formation, Int. J. Miner. Metall. Mater **24**, 550–556 (2017). DOI: 10.1007/s12613-017-1436-z
26. M. Schneider, Laser cladding with powder – effect of some machining parameters on clad properties, 1998, p. 177
27. A. Ossowska, A. Zielinski, M. Buczek, Properties of surface layers of titanium alloy TI6AL4V after laser melting processes, Adv. Mater. Sci. **10**, 63–68 (2011). DOI: 10.2478/v10077-010-0018-9
28. A.J. Gant, M.G. Gee, Structure–property relationships in liquid jet erosion of tungsten carbide hardmetals, Int. J. Refract. Met. Hard Mater. **27**, 332–343 (2009). DOI: 10.1016/j.ijrmhm.2008.11.013

Cite this article as: Samar Reda Al-Sayed Ali, Abdel Hamid Ahmed Hussein, Adel Nofal, Salah Ibrahim Hassab Elnaby, Haytham Elgazzar, A contribution to laser cladding of Ti-6Al-4V titanium alloy, Metall. Res. Technol. **116**, 634 (2019)